Materials Advances

ROYAL SOCIETY OF CHEMISTRY

PAPER

View Article Online
View Journal | View Issue

Cite this: *Mater. Adv.*, 2025, **6**, 8520

First-principles study of transition-metal doped $GaBiCl_2$ monolayers as magnetic topological insulators

Sophia Ren * and Xuan Luo

Received 24th August 2025,
Accepted 3rd October 2025

DOI: 10.1039/d5ma00951k

rsc.li/materials-advances

Magnetic topological insulators (MTIs) offer a pathway to dissipationless quantum and spintronic devices, but to date, their realization has been limited to extremely low temperatures. Therefore, identifying MTIs with sizable band gaps is crucial for raising the operating temperature toward practical applications. Through first-principles calculations, we present the first systematic study of transition-metal-doped $GaBiCl_2$ monolayers (X = Cu, Mn, Cr, and Mo) as a platform for high-temperature topological phases. We find that Cr doping induces a magnetic topological semimetal (MTSM), where strong Cr-3d/host hybridization collapses the global gap. In contrast, Mo doping stabilizes a ferromagnetic MTI with a nontrivial $\mathbb{Z}_2 = 1$ invariant and a robust spin–orbit coupling-induced band gap of 41.3 meV, indicating its potential for room temperature applications. The preservation of the nontrivial gap arises from relatively weak p–d hybridization between Mo-4d and host Bi-p states, which suppresses the impurity-driven gap closure seen with other dopants. These results make Mo-doped $GaBiCl_2$ a promising candidate for room temperature MTIs and a versatile platform for exploring the quantum anomalous Hall effect and next-generation spintronic devices.

1. Introduction

Harnessing quantum phenomena for next-generation technology requires materials that enable robust, energy-efficient information processing at practical temperatures.[1–3] Topologically protected phases offer dissipationless conduction channels resilient to local perturbations, making them ideal for scalable quantum and spintronic devices. Materials exhibiting the quantum anomalous Hall effect (QAHE), in particular, support topologically protected edge states suitable for low-power applications.[4,5] Achieving the QAHE at practical temperatures could thus unlock a new generation of quantum devices. However, realizing the QAHE at higher temperatures remains a grand challenge due to the lack of materials that combine robust ferromagnetism with a sizable topological band gap.[6] Magnetic topological insulators (MTIs), which combine topological properties with intrinsic magnetism to break time-reversal symmetry while preserving nontrivial band topology,[7–17] represent a promising route. There were many attempts to realize the QAHE in 3-dimensional (3D) MTIs, including $MnBi_2Te_4$[18] and $MnBi_2Te_4$ thin flakes,[19,20] Cr-doped $(Bi,Sb)_2Te_3$ films,[21] $MnBi_4Te_7$, $MnBi_6Te_{10}$, and $EuSn_2AS_2$,[22] all of which failed to be applicable beyond 2 K, with global band gaps of the aforementioned materials being limited below 0.2 eV. Thus, the search for magnetic topological insulators,[23–26] particularly those with sufficient bulk gaps, has emerged as a key objective in the field of topological material research. The most notable progress in 3D MTIs has been seen in $MnBi_2Te_4$-based heterostructures, where inserting a topological insulator spacer induces interlayer ferromagnetism with a predicted Curie temperature of up to 42 K and a nontrivial band gap of about 0.2 eV.[27,28] Recently, however, researchers have increasingly turned to two-dimensional (2D) materials as monolayer MTIs are more promising than their 3D counterparts for several reasons. In 2D systems, the reduced dimensionality enables robust edge states with quantized conductance, which are protected by topological invariants and less prone to backscattering or localization compared to the surface states, and they do not face challenges such as increased complexity of surface state manipulation and sensitivity to bulk defects.[29,30] This enhanced stability is critical for achieving dissipationless transport channels ideal for spintronic and quantum computing applications.

2D MTIs have garnered attention due to their unique electronic properties and promising applications. Monolayer materials such as transition metal dichalcogenides (TMDs) and halides exhibit robust topological phases, making them strong candidates for dissipationless transport.[31–33] In 2018, Baidya *et al.* demonstrated that monolayer CrI_3 can host tunable Chern insulating states.[34] The QAHE has also been realized in various monolayer systems, including the V_2MX_4 (M = W and Mo; X = Se and S) family,[35] and honeycomb–Kagome vanadium oxides,[36] which exhibit sizable topological band gaps and high Curie temperatures,

National Graphene Research and Development Center, Springfield, Virginia 22151, USA. E-mail: sophia.ren.23@gmail.com

making them viable for practical applications.[30,37–39] However, these materials face challenges in either experimental realization, magnetic stability, or synthesis. Overall, progress in 2D MTIs has been limited, primarily due to their small band gaps, the lack of extensive research on their ferromagnetic properties and the lack of intrinsically magnetic 2D MTIs.

Recent efforts have been directed at addressing these limitations by engineering 2D materials with both large topological band gaps and robust ferromagnetism. Numerous studies have explored 2D topological insulators (TIs) with large band gaps to enable their viability for room-temperature applications, including silicene,[40] germanene,[41] and stanene,[42] with reported nontrivial band gaps ranging from 1 meV to 0.3 eV. Theoretical predictions have proposed several candidates for magnetic topological insulators, such as $FeBr_3$[43] and Janus monolayers;[44] however, few showed the potential for realistic applications. A major breakthrough came with the theoretical prediction of a V_2O_3 monolayer as an intrinsic magnetic topological insulator, exhibiting a sizable nontrivial band gap (0.45 eV) as a room temperature MTI.[36] These developments set the stage for introducing our proposed material. The $GaBiCl_2$ monolayer was theoretically predicted to be a large gap topological insulator in 2015, but the effect of ferromagnetism on this material is yet to be investigated.[45]

First-principles calculations predict that $GaBiCl_2$ hosts a large nontrivial band gap ($\sim$0.65 eV) and stability due to the absence of under-coordinated atoms, making it a promising platform for higher-temperature applications.[45] A subsequent theoretical work by Maciel *et al.* demonstrated that $GaBiCl_2$ exhibits out-of-plane ferroelectric polarization with a switchable direction, enabling bistable electronic states.[46] They also found that the bandgap of $GaBiCl_2$ can be tuned by external electric fields, allowing for control over its semiconducting properties and making it suitable for applications in non-volatile memory and nanoelectronic devices. Importantly, Hangyu Li and Zhongyao Li predicted quantum edge states in $GaBiCl_2$ nanoribbons and found that vacancies in chloridized gallium bismuthide ($GaBiCl_2$) nanoribbons, especially those at the center of the nanoribbon, induce quasi-periodic scattering of these states, which may serve as a distinctive signature for defect identification.[47] Its large intrinsic band gap makes $GaBiCl_2$ an ideal platform for transition metal doping, offering the potential to break time-reversal symmetry and realize magnetic topological insulating phases. However, the effects of transition metal (TM) doping on its electronic and topological properties are yet to be investigated, prompting us to examine the TM-doped $GaBiCl_2$ monolayer.

In this study, we used density functional theory (DFT) to investigate the electronic, magnetic, and topological properties of $GaBiCl_2$ monolayers doped with transition metals (Cu, Mn, Cr, and Mo). We calculated the band structures and computed the $\mathbb{Z}_2$ topological invariant of these compounds. Finally, we compared our results to other similar research and discussed future work.

2. Methodology

We performed first-principles calculations based on density functional theory (DFT) using the projector augmented-wave (PAW) method,[48,49] as implemented in the ABINIT software package,[50] which solves the Kohn–Sham equations.[51] The exchange–correlation interaction was modeled using the Perdew–Burke–Ernzerhof (PBE) generalized gradient approximation (GGA)[52] and the pseudopotential in projector augmented wave (PAW) method.[48,49]

The plane-wave energy cutoff, vacuum, and k-point mesh were converged for each system. For TM-doped $GaBiCl_2$, the kinetic energy cutoffs for the individual components, namely, $GaBiCl_2$ and bulk TM, were determined separately, and the larger was implemented. The self-consistent field (SCF) convergence criterion was set such that the difference in total energy between two consecutive iterations was less than 1.0×10^{-10} Ha twice. The convergence parameters were converged until the energy difference between successive datasets did not exceed 1.0×10^{-4} Ha twice.

Structural optimization was carried out using the Broyden–Fletcher–Goldfarb–Shanno (BFGS) minimization method. For unit cell calculations, Brillouin zone integration was sampled using an $8 \times 8 \times 1$ k-point grid, with a shift of (0, 0, 1/2). Atomic positions were relaxed until forces on all atoms fell below 5.0×10^{-5} Ha $Bohr^{-1}$.

Using the relaxed structures, spin-polarized calculations (SPCs) were performed to compute spin-up and spin-down band structures and total magnetization, except for pristine $GaBiCl_2$ as it is nonmagnetic. Additionally, band structures incorporating and not incorporating spin–orbit coupling (SOC) were evaluated for all materials. Fig. 1(a) shows the honeycomb crystal structure of $GaBiCl_2$, and its Brillouin zone marked with chosen high-symmetry points is shown in Fig. 1(b). Doping of $GaBiCl_2$ was performed *via* substitutional doping, as shown in Fig. 1(c) and (d), where a single Cl atom was replaced with the dopant (X = Cu, Mn, Cr, and Mo) atom in a 2×2 supercell. We selected the Cl site for substitution since replacing an anion preserves the Ga–Bi framework and minimizes structural disruption, while effectively introducing carriers and magnetism without destabilizing the host lattice. The global band gap was defined as the energy difference between the conduction band minimum and the valence band maximum. Bands were plotted through the selected high-symmetry k-points in the reciprocal space, M (1/2, 0, 0), Γ (0, 0, 0), K (2/3, 1/3, 0), and back to Γ (0, 0, 0) in the first Brillouin zone of reciprocal space. The $\mathbb{Z}_2$ topological invariant was computed using Z2Pack[53,54] based on maximally localized Wannier functions obtained from ABINIT using Wannier90.[55]

3. Results

We computed the band structures of TM-doped $GaBiCl_2$ with SOC, without SOC, with SPC, and with partial density of states (DOS) under relaxed lattice parameters and examined their atomic and electronic properties. Then, we used the band structure with SOC and $\mathbb{Z}_2$ calculations to evaluate their topological characteristics.

3.1. $GaBiCl_2$

Fig. 1(c) shows the crystal structure of pristine monolayer $GaBiCl_2$. The fully relaxed optimized structure has an optimized

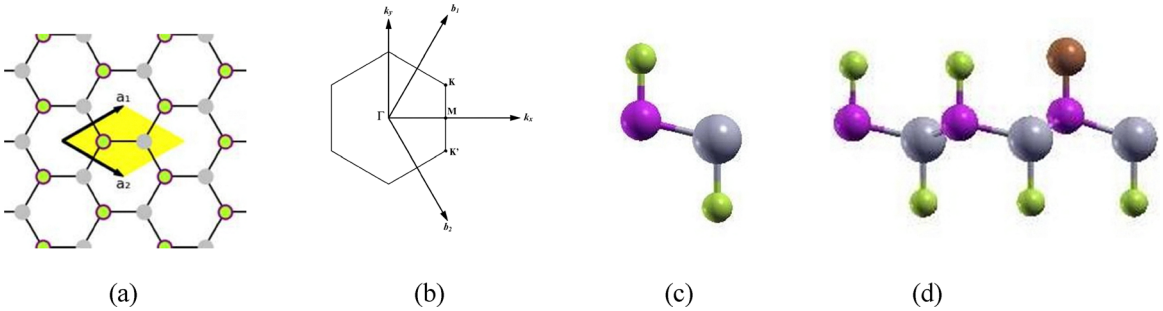

Fig. 1 (a) Honeycomb crystal structure of $GaBiCl_2$; yellow denotes the primitive cell. Green, pink, and grey represent the Cl, Ga, and Bi atoms, respectively. (b) First Brillouin zone of $GaBiCl_2$ with reciprocal vectors and high-symmetry k-points. Γ is located at the origin. (c) Side-view of the atomic structure of the $GaBiCl_2$ primitive cell. (d) Side view of the doped $GaBiCl_2$ 2 × 2 supercell, with brown representing the dopant (X).

lattice constant of a = 4.769 Å. All bond lengths and lattice constants are shown in Table 1. The electronic structures show high resemblance to those in previous studies.[45] The band structure in the absence of SOC is depicted in Fig. 2(a). The valence and conduction bands touch solely at the Γ point, thereby classifying the material as a semimetal. Under SOC, $GaBiCl_2$ becomes an insulator, as shown in Fig. 2(b). The valence band maximum shifts from the Γ point, and there are a global indirect band gap of 0.647 eV and a direct gap of 0.943 eV at the Γ point, with signs of band inversion similar to the reports for the halogenated germanene and stanene.[42,56] This band inversion is a key indicator of topological insulators, which is confirmed in Fig. 2(c) where the $\mathbb{Z}_2$ invariant is found to be 1.[57] These results agree with previous studies.[45] These large topological nontrivial band gaps will not only well exceed the thermal energy at room temperature (approximately 0.026 eV) but also decrease the transverse localization length of the edge states.[58]

The $GaBiCl_2$ monolayer's large topologically nontrivial band gap can help minimize the transverse localization length of edge states.[58] Previous studies have confirmed pristine $GaBiCl_2$ to be chemically stable, making it a suitable material for transition-metal doping.[45,47] Although experimentally difficult to confirm, it is worth mentioning that buckled honeycomb monolayer bismuth has long been predicted to act as an insulator with the QAHE.[59] Researchers have also reported that bismuth on a SiC substrate is both stable and an insulator with the QAHE and a record-high band gap of 0.8 eV.[60] When doped, the buckling height increases in the local cell where the dopant is introduced, suggesting good local structural stability around the dopant site. Therefore, TM-doped $GaBiCl_2$ is likely to be a viable and stable material for realization.

Table 1 The structural parameters of fully relaxed zigzag honeycomb configurations for pristine $GaBiCl_2$ and $Ga_4Bi_4Cl_7X_1$ (X = Cr, Cu, Mn, and Mo), including lattice constants a, buckling heights d_z, and local bond lengths in Å

X	d_z	a	d_{Ga-Bi}	d_{Bi-Cl}	d_{Ga-X}
None	0.669	4.769	2.833	2.455	2.198
Cr	1.021	9.439	2.841	2.471	2.393
Cu	0.915	9.484	2.811	2.463	2.269
Mn	1.010	9.455	2.844	2.468	2.342
Mo	1.105	9.416	2.859	2.472	2.432

3.2. Cu-doped $GaBiCl_2$

Fig. 3(a) shows the crystal structure of the Cu-doped $GaBiCl_2$ with a lattice constant of 9.484 Å after relaxation. There is a minimal structural deviation from the undoped system and the host lattice symmetry is preserved. Fig. 3(b) shows the band structure of Cu-doped $GaBiCl_2$ without SOC, which has a small global gap of 29.9 meV. However, copper doping failed to induce magnetism, as shown in Table 2, where the magnetic moment is 0 μ_B. The strong overlap between spin-up and spin-down bands in Fig. 3(c) confirms the absence of spin polarization and magnetism. This denotes a diamagnetic response, consistent with Cu's filled $3d^{10}$ configuration.[61] As a result, the system is a trivial insulator.

3.3. Mn-doped $GaBiCl_2$

The relaxed crystal structure of the Mn-doped $GaBiCl_2$ with negligible structure distortion is shown in Fig. 4(a). Mn-doped $GaBiCl_2$ produced a strong magnetic moment with multiple crossings between spin-up and spin-down bands shown in Fig. 4(e), suggesting broken time-reversal symmetry, indicative of the emergence of the QAHE. Fig. 4(b) and (c) show that upon introducing SOC, a very small indirect gap of 11.1 meV opens in the system. This gap is noticeably smaller than that found in pristine $GaBiCl_2$, likely due to magnetic resonant scattering introduced by Mn, which opens a large gap in the surface states but suppresses the long-range magnetic order required for a robust QAHE phase, a phenomenon also observed in Mn-doped Bi_2Se_3, where similar scattering effects open a surface gap without strong, homogeneous ferromagnetic alignment.[62,63]

In addition, Mn-3d orbitals introduce localized impurity states within the gap, reducing the effective insulating behavior and contributing to gap narrowing.[64] Band narrowing can also be attributed to strong p–d hybridization between Bi-p and Mn-d orbitals around the Fermi level, as shown in Fig. 4(e), which was also seen in Mn-doped Bi_2Se_3.[65] This hybridization can also make the material topologically trivial, an effect previously observed in $CaMn_2Bi_2$.[64,66,67] Consequently, despite its strong magnetization (4.5 μ_B), Mn-doped $GaBiCl_2$ is a trivial insulator,

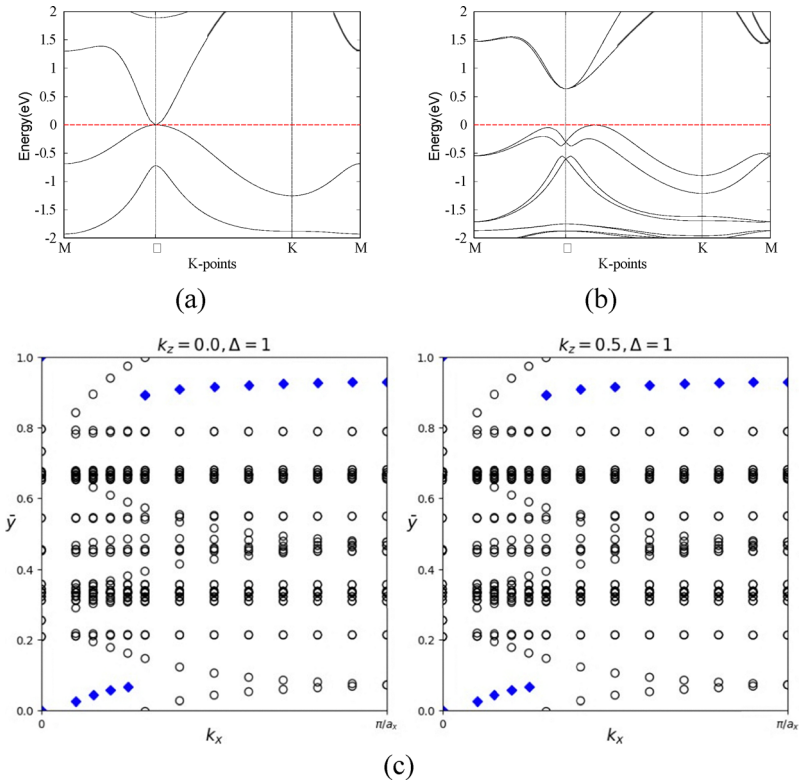

Fig. 2 The band structure of $GaBiCl_2$ (a) without SOC and (b) with SOC. (c) Time evolution of Wannier charge centers (WCCs) at k_z = 0 and k_z = 0.5. The Fermi level is set to 0 eV (dashed line). SOC opens a substantial nontrivial band gap at the Γ point and the band structure displays band inversion.

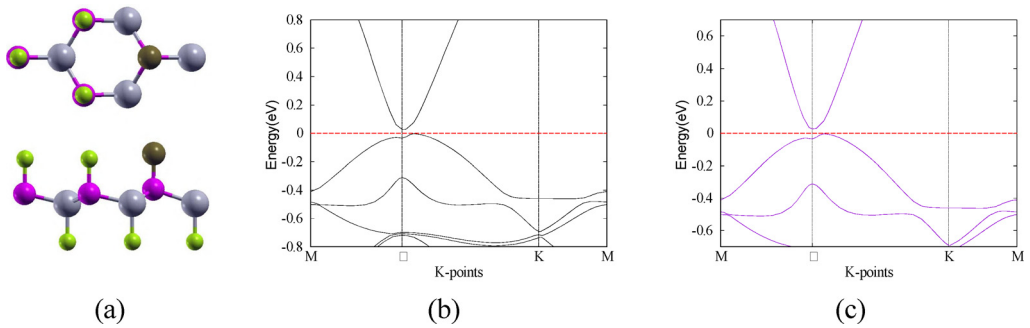

Fig. 3 Cu-doped $GaBiCl_2$'s (a) atomic structure, top view (top) and side view (bottom), with green, pink, grey, and brown representing Cl, Ga, Bi, and Cu, respectively; (b) band structure without SOC; and (c) spin-polarized band structure. Black and purple lines denote spin-up and spin-down bands, respectively. The Fermi level is set to 0 eV (dashed line). Cu doping introduced no magnetism.

as confirmed by $\mathbb{Z}_2 = 0$ from WCC analysis shown in Fig. 4(f). This trivialization likely stems from strong p–d hybridization that collapses the inverted gap.

Table 2 Each TM-doped $GaBiCl_2$ system's magnetization, in μ_B, global band gap under SOC (E_g) in eV, and classification

Dopant	Total magnetic moment (μ_B)	E_g (eV)	Classification
Mo	5.09	0.041	MTI
Cr	4.92	0.000	MTSM
Mn	4.52	0.011	Trivial insulator
Cu	0.00	—	Trivial insulator
None	0.00	0.647	TI

3.4. Cr-doped $GaBiCl_2$

Cr-doped $GaBiCl_2$ also demonstrated little structural deviation from the pristine system, as shown in Fig. 5(a), with electronic structures demonstrating similar characteristics to the Mn-doped system. This can be attributed to the comparable 3d orbital occupancies of Cr and Mn, which lead to analogous exchange splitting and hybridization with surrounding p-orbitals of Bi, as shown in Fig. 5(d). However, unlike the Mn-doped system, Cr-doped $GaBiCl_2$ exhibits a semimetallic state under SOC, where the conduction band, although not crossing with the valence bands, dips below the Fermi level for band structures both with and without SOC, as shown in Fig. 5(b)

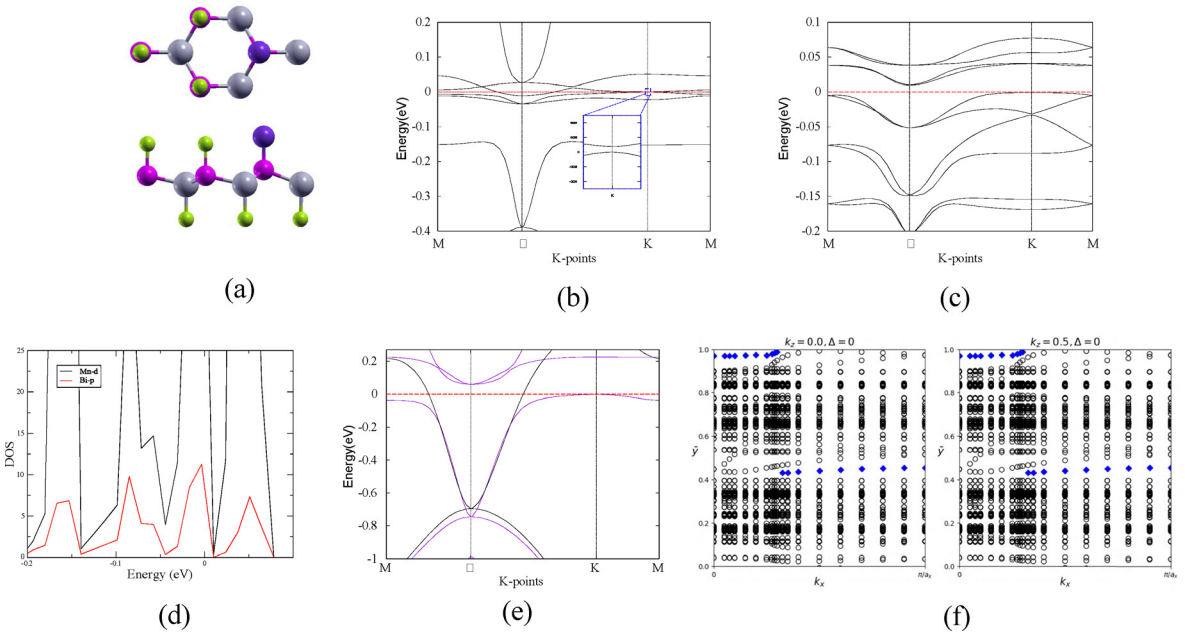

Fig. 4 Mn-doped $GaBiCl_2$'s (a) atomic structure, top view (top) and side view (bottom), with green, pink, grey, and purple representing Cl, Ga, Bi, and Mn, respectively; (b) band structure without SOC; (c) band structure with SOC; (d) projected partial DOS on the dopant and the neighboring Bi atom; (e) spin-polarized band structure; and (f) time evolution of Wannier charge centers (WCCs) at $k_z = 0$ and $k_z = 0.5$. The Fermi level is set to 0 eV (dashed line). Black and purple lines denote the spin-up and spin-down bands, respectively.

and (c). Notably, after the inclusion of SOC, band degeneracies are preserved only at the Γ point. This localized degeneracy is a direct consequence of the underlying crystalline symmetry and remaining inversion symmetry at that high-symmetry point. Away from Γ, the degeneracies are lifted likely due to the combined effects of ferromagnetic exchange interactions and SOC, indicating that TRS is broken across the Brillouin zone. Like Mn-doped $GaBiCl_2$, band narrowing can be attributed to strong p–d hybridization between Bi-p and Cr-d orbitals, which was also seen in Cr-doped Bi_2Se_3.[65] In addition, the collapse of

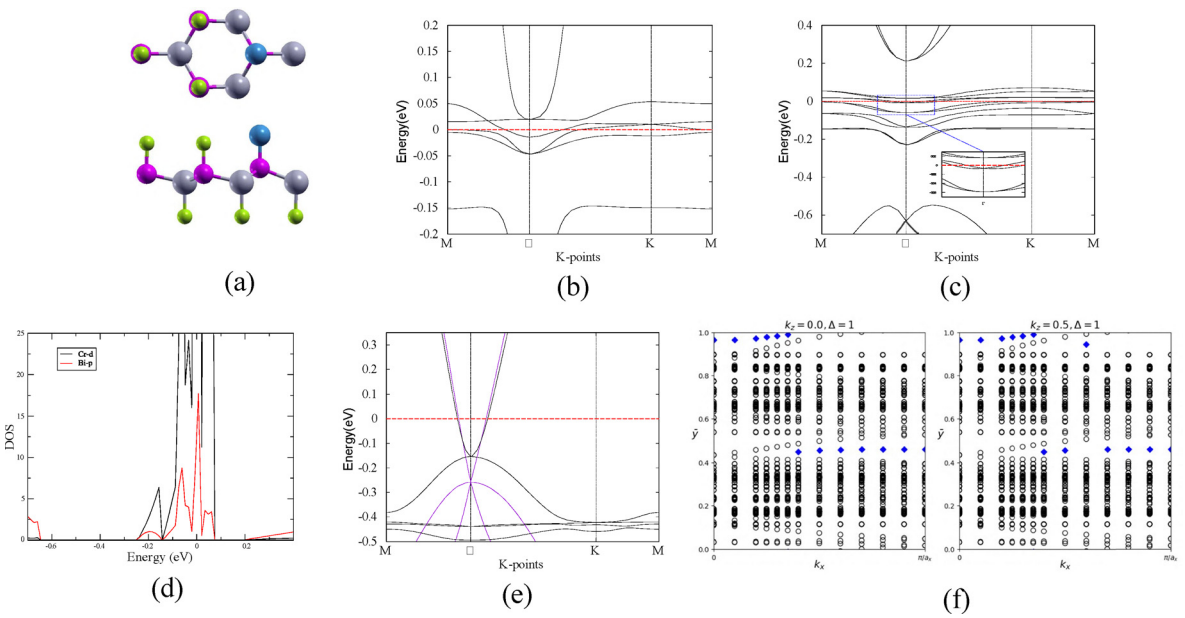

Fig. 5 Cr-doped $GaBiCl_2$'s (a) atomic structure, top view (top) and side view (bottom), with green, pink, grey, and blue representing Cl, Ga, Bi, and Cr, respectively; (b) band structure without SOC; (c) band structure with SOC; (d) projected partial DOS on the dopant and the neighboring Bi atom; (e) spin-polarized band structure; and (f) time evolution of Wannier charge centers (WCCs) at $k_z = 0$ and $k_z = 0.5$. Black and purple lines denote spin-up and spin-down bands, respectively. The Fermi level is set to 0 eV (dashed line). Cr doping induces a semimetallic phase with strong exchange splitting and maintains topological order.

the band gap in Cr-doped $GaBiCl_2$ may also be attributed to Fermi level pinning. Chromium's partially filled 3d orbitals can introduce mid-gap states or defect-like electronic states that energetically align near the Fermi level. These states effectively shift the Fermi level into the conduction band, creating semimetallic character despite the preservation of topological order. This mechanism has been previously observed in other TM-doped topological systems, such as Sn-doped Bi_2Te_2Se and Ag-doped Bi_2Se_3, where localized defect states interfere with global band gap formation.[68,69] Chromium doping results in a magnetic moment of 4.92 μ_B, shown in Table 2, and induces strong spin polarization in the electronic structure, leading to the exchange splitting of the spin-up and spin-down bands near the Fermi level in Fig. 5(e). The conduction band dipping below the Fermi level leads to electron pockets, while the valence band contributes hole pockets, maintaining the topological nontrivial phase at the surfaces $k_z = 0$ and $k_z = 0.5$, as shown in Fig. 5(f).

Although WCC evolution indicates a retained nontrivial topology, the absence of a global gap makes Cr-doped $GaBiCl_2$ a magnetic topological semimetal (MTSM). External tuning through strain, gating, or chemical substitution may reopen the gap, enabling a controllable MTSM–MTI transition. A precedent for such a transition is seen in $(Mn_{1-x}Sn_x)Bi_2Te_4$, where Sn doping initially collapses the band gap into a semimetallic phase, but at higher concentrations, reopens it into a MTI.[70] By analogy, tuning parameters such as the chemical composition, strain, or layer thickness may stabilize an insulating phase in Cr-doped $GaBiCl_2$. This makes the material a strong candidate for further exploration in MTSM-to-MTI transition.

3.5. Mo-doped $GaBiCl_2$

Fig. 6(a) shows the atomic structure of Mo-doped $GaBiCl_2$, with a large buckling height in the local cell of the dopant shown in Table 1, signaling a rather strong bonding strength between Ga and Mo. In contrast to the Cr-doped case, Mo-doped $GaBiCl_2$ does develop a significant band gap. The band structure without SOC is shown in Fig. 6(b), showing a small gap of 0.001 eV opening at the k point. Upon introducing SOC, a direct band gap of 0.140 eV appears at the Γ point and, crucially, a global indirect band gap of 41.3 meV remains, as shown in Fig. 6(c). The 41.3 meV gap well exceeds the gap needed for room temperature, namely, 0.026 eV, and Mo-doped $GaBiCl_2$ is therefore anticipated to be a room-temperature magnetic topological insulator. This value is comparable to that of the most optimistic theoretical candidates such as Kagome-based systems and significantly larger than that of the gaps observed in prototypical MTIs such as Cr-doped $(Bi,Sb)_2Te_3$ or $MnBi_2Te_4$, where exchange gaps are only a few meV.[19,21,34–36,71] The characteristic band inversion at the Γ point is preserved after Mo doping, indicative of topological nontrivial order.

Mo's success in preserving a band gap is likely due to the fact that Mo's 4d electrons, unlike other the 3d electrons of the other dopants used in this study, hybridize more weakly with Bi-p states around the Fermi level, as shown in Fig. 6(d), preventing impurity-induced gap closure.[64] It is noteworthy that the 2D material $MoTe_2F_2$ has recently been predicted to

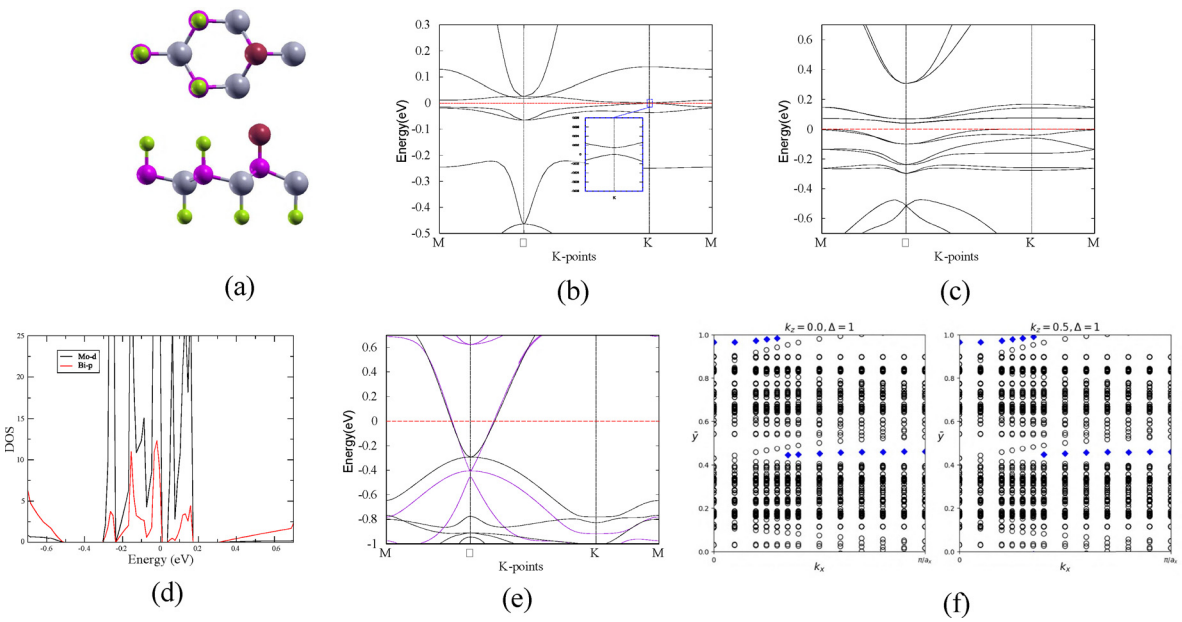

Fig. 6 Mo-doped $GaBiCl_2$'s (a) atomic structure, top view (top) and side view (bottom), with green, pink, grey, and red representing Cl, Ga, Bi, and Mo, respectively; (b) band structure without SOC; (c) band structure with SOC; (d) projected partial DOS on the dopant and the neighboring Bi atom; (e) spin-polarized band structure; and (f) time evolution of Wannier charge centers (WCCs) at $k_z = 0$ and $k_z = 0.5$. Black and purple lines denote spin-up and spin-down bands, respectively. The Fermi level is set to 0 eV (dashed line). Mo doping preserves a large topologically nontrivial band gap while introducing strong magnetism and band splitting.

exhibit both a quadruple band crossing-induced high-performing QAHE and a large band gap.[72] Meanwhile, Mo-doping also successfully introduces ferromagnetism to the material with a strong magnetic moment, shown in Table 2, and evidence of strong band-splitting under spin-polarization, shown in Fig. 6(e). The emergence of a band gap alongside robust ferromagnetism confirms that time-reversal symmetry is broken in the system. Yet, this symmetry breaking does not disrupt its topology, as our $\mathbb{Z}_2$ calculations reveal that the system retains its topologically non-trivial phase, characterized by $\mathbb{Z}_2 = 1$, at the surfaces with $k_z = 0$ and $k_z = 0.5$, as shown in Fig. 6(f). Overall, Mo-doped $GaBiCl_2$ is a room-temperature MTI that is promising for spintronic applications and as a platform for realizing the QAHE at higher temperatures.

In this context, external tuning parameters such as strain, electric gating, and correlation strength provide promising routes to further enhance the topological phases. Recently, across diverse systems, these strategies have enabled either the stabilization of QAHE phases or the enlargement of topological gaps: stacking and strain modulation can generate altermagnetism with spin-split states even without net magnetization,[73] while strain- or correlation-driven tuning has enhanced the nontrivial band gap in $LaPdO_3$ and $LaPtO_3$ bilayers,[74] and group-IV monochalcogenides have exhibited multiple Hall effects controllable by strain and built-in fields, with reported gaps in the range of several tens of meV.[75] Recently, silicene on SiC was presented as a potential 2D candidate for realizing the QAHE with a reported band gap of 1.3 meV.[76] By comparison, Mo-doped $GaBiCl_2$ exhibits a robust gap of 41.3 meV, performing comparable to the recent leading 2D candidates, such as $LaPtO_3$ bilayers and $VSiSnN_4$.[73–76] Interestingly, in $LaPdO_3$, compressive in-plane strain increased the QAHE gap from 92 meV to 242 meV.[74] Given this precedent, Mo-doped $GaBiCl_2$ leaves open the possibility of further enlargement under external tuning, potentially positioning it alongside the most competitive candidates for high-temperature QAHE. For Cr-doped $GaBiCl_2$, such strategies may provide a pathway to reopen the collapsed gap and drive the system from its present semimetallic state toward a true QAHE phase.

4. Conclusions

Through first-principles investigations, we have theoretically predicted the emergence of topologically nontrivial and ferromagnetic phases in Mo-doped and Cr-doped $GaBiCl_2$ monolayers. Pristine $GaBiCl_2$ is a topological insulator. Upon doping, spin-polarized calculations reveal that substituting a Cl atom with Cr or Mo introduces strong magnetism. Among them, Mo-doped $GaBiCl_2$ exhibits both a robust ferromagnetic ground state and a SOC-induced global room-temperature band gap of 41.3 meV, accompanied by band inversion and a nontrivial $\mathbb{Z}_2$ invariant, firmly establishing it as a magnetic topological insulator and placing Mo–$GaBiCl_2$ among the most promising MTI candidates reported to date. Although Cr-doped $GaBiCl_2$ retains the nontrivial topology, it lacked an bulk gap, yielding a magnetic topological semimetal state. Due to its proximity to an insulating phase, Cr-doped $GaBiCl_2$ is an intriguing platform for exploring transitions from an MTSM to an MTI *via* external tuning. The combination of an insulating gap and intrinsic ferromagnetism in Mo-doped $GaBiCl_2$ makes it a prime candidate for next-generation spintronic devices and a platform for further research and realizing the quantum anomalous Hall effect at elevated temperatures. Future research should assess the Curie temperature and stability of Mo-doped $GaBiCl_2$, while exploring strain or chemical tuning to enlarge its gap and guide experimental realization toward practical spintronic and QAHE devices.

Conflicts of interest

There are no conflicts to declare.

Data availability

Data for this article, including input files, output files, raw data, and figures, are available at figshare at **https://doi.org/10.6084/m9.figshare.29924957.v1**, **https://doi.org/10.6084/m9.figshare.29924936**, **https://doi.org/10.6084/m9.figshare.29974192**, **https://doi.org/10.6084/m9.figshare.29974168** and **https://doi.org/10.6084/m9.figshare.29924933**.

References

1 N. P. De Leon, K. M. Itoh, D. Kim, K. K. Mehta, T. E. Northup, H. Paik, B. Palmer, N. Samarth, S. Sangtawesin and D. W. Steuerman, *Science*, 2021, **372**, 2823.
2 X. Liu and M. C. Hersam, *Nat. Rev. Mater.*, 2019, **4**, 669.
3 V. Lordi and J. M. Nichol, *MRS Bull.*, 2021, **46**, 589.
4 J. Wang, B. Lian and S.-C. Zhang, *Phys. Scr.*, 2015, 014003.
5 K. He, Y. Wang and Q.-K. Xue, *Annu. Rev. Condens. Matter Phys.*, 2018, **9**, 329.
6 Y. Tokura, K. Yasuda and A. Tsukazaki, *Nat. Rev. Phys.*, 2019, **1**, 126.
7 X.-L. Qi, Y.-S. Wu and S.-C. Zhang, *Phys. Rev. B: Condens. Matter Mater. Phys.*, 2006, **74**, 085308.
8 C.-X. Liu, X.-L. Qi, X. Dai, Z. Fang and S.-C. Zhang, *Phys. Rev. Lett.*, 2008, **101**, 146802.
9 C.-X. Liu, S.-C. Zhang and X.-L. Qi, *Annu. Rev. Condens. Matter Phys.*, 2016, **7**, 301.
10 X. Kou, Y. Fan, M. Lang, P. Upadhyaya and K. L. Wang, *Solid State Commun.*, 2015, **215**, 34.
11 Y. Chen, J. G. Analytis, J.-H. Chu, Z. Liu, S.-K. Mo, X.-L. Qi, H. Zhang, D. Lu, X. Dai and Z. Fang, *et al.*, *Science*, 2009, **325**, 178.
12 D. Hsieh, D. Qian, L. Wray, Y. Xia, Y. S. Hor, R. J. Cava and M. Z. Hasan, *Nature*, 2008, **452**, 970.
13 T. Zhang, P. Cheng, X. Chen, J.-F. Jia, X. Ma, K. He, L. Wang, H. Zhang, X. Dai and Z. Fang, *et al.*, *Phys. Rev. Lett.*, 2009, **103**, 266803.

14 K. Nomura and N. Nagaosa, *Phys. Rev. Lett.*, 2011, **106**, 166802.
15 M. Mogi, R. Yoshimi, A. Tsukazaki, K. Yasuda, Y. Kozuka, K. Takahashi, M. Kawasaki and Y. Tokura, *Appl. Phys. Lett.*, 2015, **107**, 182401.
16 F. Wang, Y.-F. Zhao, Z.-J. Yan, D. Zhuo, H. Yi, W. Yuan, L. Zhou, W. Zhao, M. H. Chan and C.-Z. Chang, *Nano Lett.*, 2023, **23**, 2483.
17 T.-M. T. Tran, D.-A. Le, T.-M. Pham, K.-T. T. Nguyen and M.-T. Tran, *Phys. Rev. B*, 2020, **102**, 205124.
18 M. M. Otrokov, *et al.*, *Nature*, 2019, **576**, 416.
19 C. Liu, Y. Wang, H. Li, Y. Wu, Y. Li, J. Li, K. He, Y. Xu, J. Zhang and Y. Wang, *Nat. Mater.*, 2020, **19**, 522.
20 Y. Deng, Y. Yu, M. Z. Shi, Z. Guo, Z. Xu, J. Wang, X. H. Chen and Y. Zhang, *Science*, 2020, **367**, 895.
21 C.-Z. Chang, J. Zhang, X. Feng, J. Shen, Z. Zhang, M. Guo, K. Li, Y. Ou, P. Wei and L.-L. Wang, *et al.*, *Science*, 2013, **340**, 167.
22 H. Li, S.-Y. Gao, S. F. Duan, Y. F. Xu, K.-J. Zhu, S.-J. Tian, J.-C. Gao, W.-H. Fan, Z.-C. Rao and J.-R. Huang, *et al.*, *Phys. Rev. X*, 2019, **9**, 041039.
23 J.-Y. You, Z. Zhang, B. Gu and G. Su, *Phys. Rev. Appl.*, 2019, **12**, 024063.
24 J. Sun, X. Zhong, W. Cui, J. Shi, J. Hao, M. Xu and Y. Li, *Phys. Chem. Chem. Phys.*, 2020, **22**, 2429.
25 Y. Li, J. Li, Y. Li, M. Ye, F. Zheng, Z. Zhang, J. Fu, W. Duan and Y. Xu, *Phys. Rev. Lett.*, 2020, **125**, 086401.
26 Y. Tokura, *Nat. Rev. Phys.*, 2023, **5**, 439.
27 S. Qi, R. Gao, M. Chang, Y. Han and Z. Qiao, *Phys. Rev. B*, 2020, **101**, 014423.
28 D. Zhang, M. Shi, T. Zhu, D. Xing, H. Zhang and J. Wang, *Phys. Rev. Lett.*, 2019, **122**, 206401.
29 Z.-X. Li and H. Yao, *Phys. Rev. B*, 2017, **96**, 241101.
30 L. Kou, Y. Ma, Z. Sun, T. Heine and C. Chen, *J. Phys. Chem. Lett.*, 2017, **8**, 1905.
31 K. Carva, J. Kudrnovsky, F. Maca, V. Drchal, I. Turek, P. Balaz, V. Tkac, V. Holy, V. Sechovsky and J. Honolka, *Phys. Rev. B*, 2016, **93**, 214409.
32 Z. Li, P. Zhou, Q. Yan, X. Peng, Z. Ma and L. Sun, *Phys. Rev. B*, 2022, **106**, 085126.
33 Q. Ruan, W. Lei, G. Cuono, C. Autieri, K. Xu, X. Gong, W. Wang and X. Ming, *Appl. Phys. Lett.*, 2024, **125**, 143102.
34 S. Baidya, J. Yu and C. H. Kim, *Phys. Rev. B*, 2018, **98**, 155148.
35 Y. Jiang, H. Wang, K. Bao, Z. Liu and J. Wang, *Phys. Rev. Lett.*, 2024, **132**, 106602.
36 S. Mellaerts, R. Meng, M. Menghini, V. Afanasiev, J. W. Seo, M. Houssa and J.-P. Locquet, *npj 2D Mater. Appl.*, 2021, **5**, 65.
37 V. Fatemi, S. Wu, Y. Cao, L. Bretheau, Q. D. Gibson, K. Watanabe, T. Taniguchi, R. J. Cava and P. Jarillo-Herrero, *Science*, 2018, **362**, 926.
38 L.-Y. Feng, R. A. B. Villaos, H. N. Cruzado, Z.-Q. Huang, C.-H. Hsu, H.-C. Hsueh, H. Lin and F.-C. Chuang, *Chin. J. Phys.*, 2020, **66**, 15.
39 H. P. Wang, W. Luo and H. J. Xiang, *Phys. Rev. B*, 2017, **95**, 125430.
40 P. Vogt, P. De Padova, C. Quaresima, J. Avila, E. Frantzeskakis, M. C. Asensio, A. Resta, B. Ealet and G. Le Lay, *Phys. Rev. Lett.*, 2012, **108**, 155501.
41 C.-C. Liu, W. Feng and Y. Yao, *Phys. Rev. Lett.*, 2011, **107**, 076802.
42 Y. Xu, B. Yan, H.-J. Zhang, J. Wang, G. Xu, P. Tang, W. Duan and S.-C. Zhang, *Phys. Rev. Lett.*, 2013, **111**, 136804.
43 S.-H. Zhang and B.-G. Liu, *arXiv*, Preprint, arXiv:1706.08943, 2017, DOI: 10.48550/arXiv:1706.08943.
44 N.-J. Yang and J.-M. Zhang, *Phys. Rev. B*, 2024, **109**, 035423.
45 L. Li, X. Zhang, X. Chen and M. Zhao, *Nano Lett.*, 2015, **15**, 1296.
46 R. Maciel, A. Araujo, C. Lewenkopf and G. Ferreira, *Phys. Rev. B*, 2021, **103**, 205124.
47 H. Li and Z. Li, *J. Phys.: Condens. Matter*, 2023, **35**, 255302.
48 N. Holzwarth, A. Tackett and G. Matthews, *Comput. Phys. Commun.*, 2001, **135**, 329.
49 P. E. Blöchl, *Phys. Rev. B: Condens. Matter Mater. Phys.*, 1994, **50**, 17953.
50 X. Gonze, B. Amadon, P.-M. Anglade, J.-M. Beuken, F. Bottin, P. Boulanger, F. Bruneval, D. Caliste, R. Caracas and M. Cote, *et al.*, *Comput. Phys. Commun.*, 2009, **180**, 2582.
51 W. Kohn and L. J. Sham, *Phys. Rev.*, 1965, **140**, A1133.
52 J. P. Perdew, K. Burke and M. Ernzerhof, *Phys. Rev. Lett.*, 1996, **77**, 3865.
53 D. Gresch, G. Autes, O. V. Yazyev, M. Troyer, D. Vanderbilt, B. A. Bernevig and A. A. Soluyanov, *Phys. Rev. B*, 2017, **95**, 075146.
54 A. A. Soluyanov and D. Vanderbilt, *Phys. Rev. B: Condens. Matter Mater. Phys.*, 2011, **83**, 235401.
55 A. A. Mostofi, J. R. Yates, G. Pizzi, Y.-S. Lee, I. Souza, D. Vanderbilt and N. Marzari, *Comput. Phys. Commun.*, 2014, **185**, 2309.
56 C. Si, J. Liu, Y. Xu, J. Wu, B.-L. Gu and W. Duan, *Phys. Rev. B: Condens. Matter Mater. Phys.*, 2014, **89**, 115429.
57 Z. Zhu, Y. Cheng and U. Schwingenschlogl, *Phys. Rev. B: Condens. Matter Mater. Phys.*, 2012, **85**, 235401.
58 A. Marrazzo, M. Gibertini, D. Campi, N. Mounet and N. Marzari, *Nano Lett.*, 2019, **19**, 8431.
59 J.-J. Zhou, W. Feng, C.-C. Liu, S. Guan and Y. Yao, *Nano Lett.*, 2014, **14**, 4767.
60 F. Reis, G. Li, L. Dudy, M. Bauernfeind, S. Glass, W. Hanke, R. Thomale, J. Schaefer and R. Claessen, *Science*, 2017, **357**, 287.
61 S. Ramachandra Rao, *Proc. - Indian Acad. Sci., Sect. A*, 1935, **2**, 249–259.
62 J. Teng, N. Liu and Y. Li, *J. Semicond.*, 2019, **40**, 081507.
63 J. Sanchez-Barriga, A. Varykhalov, G. Springholz, H. Steiner, R. Kirchschlager, G. Bauer, O. Caha, E. Schierle, E. Weschke and A. Unal, *et al.*, *Nat. Commun.*, 2016, **7**, 10559.
64 O. Farberovich, A. Yaresko, K. Kikoin and V. Fleurov, *Phys. Rev. B: Condens. Matter Mater. Phys.*, 2008, **78**, 085206.
65 J.-M. Zhang, W. Zhu, Y. Zhang, D. Xiao and Y. Yao, *Phys. Rev. Lett.*, 2012, **109**, 266405.
66 Q. Gibson, H. Wu, T. Liang, M. Ali, N. P. Ong, Q. Huang and R. J. Cava, *Phys. Rev. B: Condens. Matter Mater. Phys.*, 2015, **91**, 085128.
67 C. Lane, M. M. Piva, P. F. S. Rosa and J.-X. Zhu, *Sci. Rep.*, 2023, **13**, 9271.

68 S. Kushwaha, Q. Gibson, J. Xiong, I. Pletikosic, A. Weber, A. Fedorov, N. P. Ong, T. Valla and R. J. Cava, *J. Appl. Phys.*, 2014, **115**, 143708.
69 T. Uchiyama, H. Goto, E. Uesugi, A. Takai, L. Zhi, A. Miura, S. Hamao, R. Eguchi, H. Ota and K. Sugimoto, *et al.*, *Sci. Rep.*, 2023, **13**, 537.
70 A. V. Tarasov, T. P. Makarova, D. A. Estyunin, A. V. Eryzhenkov, I. I. Klimovskikh, V. A. Golyashov and K. A. Kokh, *Symmetry*, 2023, **15**, 469.
71 L. Ye, M. Kang, J. Liu, F. Von Cube, C. R. Wicker, T. Suzuki, C. Jozwiak, A. Bostwick, E. Rotenberg and D. C. Bell, *et al.*, *Nature*, 2018, **555**, 638.
72 F. Chen, H. Chen, X. Zhao, G. Hu, X. Yuan and J. Ren, *Phys. Rev. B*, 2025, **111**, 075133.
73 W. Xun, X. Liu, Y. Zhang, Y.-Z. Wu and P. Li, *Appl. Phys. Lett.*, 2025, **126**, 101903.
74 H.-S. Lu and G.-Y. Guo, *Phys. Rev. B*, 2019, **99** 104405.
75 P. Li, X. Yang, Q.-S. Jiang, Y.-Z. Wu and W. Xun, *Phys. Rev. Mater.*, 2023, **7**, 064002.
76 P. Li, X. Li, W. Zhao, H. Chen, M.-X. Chen, Z.-X. Guo, J. Feng, X.-G. Gong and A. H. MacDonald, *Nano Lett.*, 2017, **17**, 6195.